Finite Elements in Analysis and Design 67 (2013) 43–55

Contents lists available at SciVerse ScienceDirect

Finite Elements in Analysis and Design

journal homepage: www.elsevier.com/locate/finel

Coupling flat-top partition of unity method and finite element method

Won-Tak Hong [a], Phill-Seung Lee [b,*]

[a] KAIST Institute for Design of Complex Systems, 291 Daehak-ro, Yuseong-gu, Daejeon 305-701, Republic of Korea
[b] KAIST Ocean Systems Engineering, 291 Daehak-ro, Yuseong-gu, Daejeon 305-701, Republic of Korea

ARTICLE INFO

Article history:
Received 30 January 2012
Received in revised form
9 October 2012
Accepted 11 December 2012

Keywords:
Coupling
Enrichment
Flat-top
Partition of unity
Finite element method

ABSTRACT

We present a novel technique of coupling finite element method with mesh-based flat-top partition of unity method. The proposed coupling method allows us to bind any order of finite elements with flat-top partition of unity method. To verify the coupling, we test the coupling method on one- and two-dimensional boundary value problems including linear elasticity problem on a cracked domain. The coupled formulation provides a platform for stable enrichments to obtain highly accurate solution especially in the enrichment area.

1. Introduction

In recent years, many partition of unity methods showed great success in the form of meshless method; element-free Galerkin method (EFGM) [1], reproducing Kernel particle method (RKPM) [2], method of finite sphere [3], and reproducing polynomial particle method (RPPM) [4] to name a few. On the other hand, partition of unity methods that use finite element mesh explicitly becomes popular in later years because of the easy applicability. h-p clouds [5], eXtended finite element method (XFEM) [6,7], and generalized finite element method (GFEM) [8] are in this category.

Recently proposed mesh-based construction of flat-top partition of unity function (MFPUM) [9], which uses finite element mesh explicitly, is inspired by a meshless enrichment technique [5,8,10–12]. Like GFEM or XFEM, MFPUM emphasized the use of finite element mesh to alleviate the difficulty in numerical integration. The main difference with GFEM or XFEM is the existence of flat-top in the partition of unity functions. MFPUM has the ability to enrich any order of polynomials locally with the Kronecker-delta property. Thus, imposing essential boundary conditions is straightforward as in finite element method. MFPUM is a promising method and has been successfully applied on problems that contain singularities to obtain highly accurate results. However, applying MFPUM on the entire computational domain may not be economical compared to FEM. It is more desirable to use the same order of finite elements over MFPUM on the region where the solution is smooth because MFPUM demands more DOFs compared to the same order of finite element method. Hence, it is worth to try to couple MFPUM and the finite element method.

Several techniques have been proposed to couple finite element method with different numerical methods, such as coupling finite element method with spectral method [13], with eXtended finite element method (XFEM) [14], with boundary element method (BEM) [15–17], with element free Galerkin method (EFGM) [18–21], and with moving least square method (MLS) [22]. However, the coupling method that is used in [13,15–20,22] is not applicable to couple higher order finite element method and partition of unity method.

In general, when coupling of two methods is considered, the computational domain is partitioned into two regions, and a method is chosen in each part where it is more appropriate. In such case, the continuity of the primary variable becomes an issue at the interface. Some of the commonly used technique to enforce the continuity requirement is the use of Lagrange multipliers and domain decomposition method. Both these techniques are powerful and scalable to be used for coupling of large systems. However, we prefer to have a coupling method without dealing an indefinite system and avoid iterations between subregions to get a coupled solution that is continuous. We see the coupling formulation given in [20] shares our point of view; however, the formulation, which uses mixed interpolation, is not suitable in our case.

In this paper, we will introduce a technique to couple arbitrary order of finite elements with MFPUM. To achieve a seamless coupling between these two, we develop transitional partition of unity function, which helps the transition. A schematic view of

* Corresponding author. Tel.: +82 42 350 1512; fax: +82 42 350 1510.
E-mail address: phillseung@kaist.edu (P.S. Lee).

0168-874X/$ - see front matter © 2012 Elsevier B.V. All rights reserved.
http://dx.doi.org/10.1016/j.finel.2012.12.002

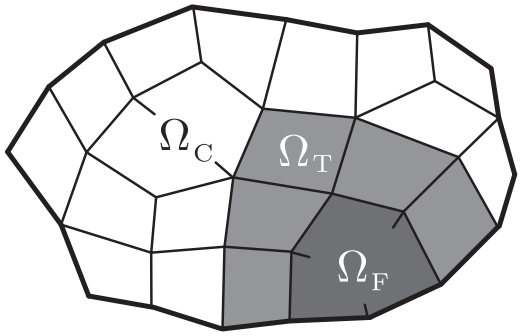

Fig. 1. Schematic partition of computational domain Ω into three parts: Ω_C where finite element is used, Ω_T where transition occurs, and Ω_F where flat-top partition of unity method is used.

such coupling in two dimensions is shown in Fig. 1. In this way, the coupled system can be dealt with a single weak form which results a positive definite system.

In the following sections, we first briefly explain mesh-based flat-top partition of unity method (MFPUM) and propose a method to couple MFPUM with FEM. To show the feasibility and effectiveness of the coupling method, we then numerically study a heat conduction problem on a bar with a boundary layer, potential flow around a cylinder and a single-edge cracked plate under uniform tension.

2. Mesh-based flat-top partition of unity method

In our previous work (MFPUM), we achieved an arbitrary order of polynomial enrichment by introducing a systematic and an efficient way of generating flat-top partition of unity functions on a *provided mesh*. Let us review the basic ideas of mesh-based flat-top partition of unity method (MFPUM) in one dimension. Let us begin by establishing some basic notations:

- *Element* E_i: A member of collection $\{E_i\}$, which partitions the domain Ω. Elements are non-overlapping, $E_i \cap E_j = \emptyset$ for $i \neq j$, and form a cover of Ω, $\bigcup_{i=1}^{N} E_i = \Omega$. In one dimension, two points ${}^{i}p_1$ and ${}^{i}p_2$ will define an element E_i. See, for example Fig. 2(a).
- *Flat-top parameter* χ_i: The flat-top size of the partition of unity function is controlled by a parameter $0 < \chi_i < 1$. Each element E_i is shrunken to E_i' by the parameter χ_i. See for example, Fig. 2(b). Each physical element E_i is defined on a local coordinate system by elemental mapping. Let T_i be the elemental mapping which maps the interval $(-1,1)$ to the element E_i. i.e. $T_i(-1) = {}^{i}p_1$ and $T_i(1) = {}^{i}p_2$. Then the mapping T_i provides the two nodes $T_i(-\chi_i) = {}^{i}p_1'$ and $T_i(\chi_i) = {}^{i}p_2'$ that defines E_i'. It is possible to control χ_i element-wise, however, we fix χ_i to be a global parameter, $\chi_i = \chi$ for $i = 1, \ldots, N$, in our numerical examples for convenience.
- *Supplemental mesh*: The interconnection between shrunken element E_i' results a supplemental mesh shown in Fig. 2(b) and will be used to build flat-top partition of unity functions. The numerical integration will be performed on the subpatches that forms supplemental mesh.
- *Patch* Q_i: A patch is a member of a covering $\{Q_i\}$, $\Omega \subset \bigcup_{i=1}^{N} Q_i$. The difference between an element E_i and a patch Q_i is that a patch can overlap with its neighboring patch(es). Fig. 2(c) shows the overlapped patches defined on the supplemental mesh. Note that the patch Q_i completely includes element E_i.
- *Partition of unity function* ϕ_i: A family of functions $\{\phi_i\}$ subordinated to each patch Q_i is called partition of unity functions if they satisfy $\sum_{i=1}^{N} \phi_i(\mathbf{x}) = 1$, $\forall \mathbf{x} \in \Omega$ where N is the total number of elements. A flat-top area of partition of unity function ϕ_i that is shown in Fig. 2(c) is given in closed form as follows:

$$\phi_i(x) = \begin{cases} \dfrac{1}{{}^{i}p' - {}^{i-1}p_2'}(x - {}^{i-1}p_2') & \text{if } x \in Q_{i-1} \backslash Q_i, \\ 1 & \text{if } x \in Q_i \backslash (Q_{i-1} \cup Q_{i+1}), \\ \dfrac{-1}{{}^{i+1}p_1' - {}^{i}p_2'}(x - {}^{i+1}p_1') & \text{if } x \in Q_{i+1} \backslash Q_i, \end{cases} \tag{1}$$

where $Q_i' = Q_i \backslash (Q_{i-1} \cup Q_{i+1})$ is the flat-top area of ϕ_i.

- *Node* ${}^{i}n_k$: The kth node of element E_i is denoted by ${}^{i}n_k$. The points $({}^{i}n_k, k = 1, \ldots, N)$ which includes the end points of the interval are distributed in the local coordinate system and then mapped to the flat-top area of the patch E_i'. Fig. 2(d) shows three nodes defined on element E_i.
- *Local approximation function* ${}^{i}L_k$: We use the Lagrange interpolating functions defined by the nodes ${}^{i}n_k$ as local approximation functions. Note that the support of Lagrange interpolating functions are unbounded, see Fig. 2(d). The local

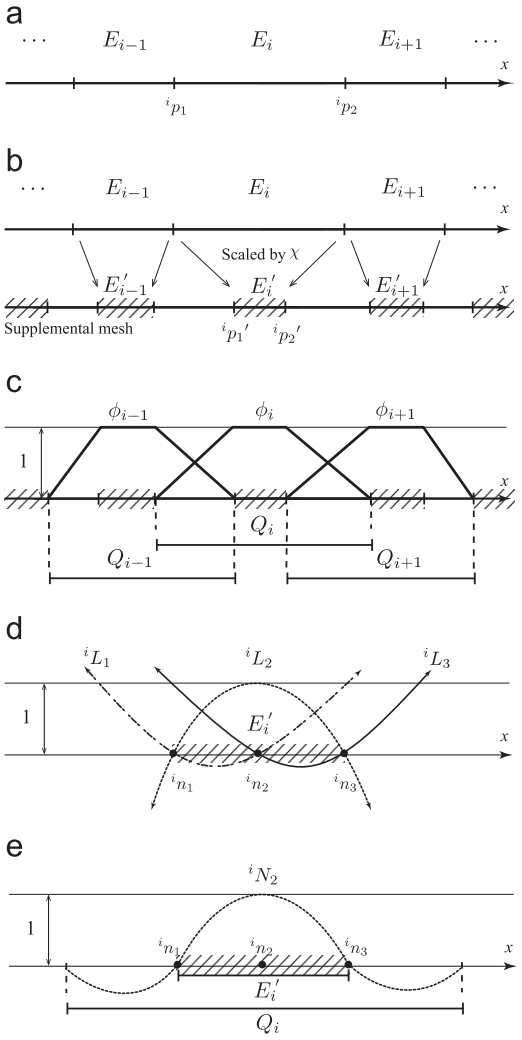

Fig. 2. MFPUM in one dimension: (a) elements and nodes; (b) shrinking elements to find flat-top regions; (c) flat-top partition of unity functions on patches; (d) second-order Lagrange interpolating functions defined by the nodes on element E_i'; (e) global quadratic approximation functions on patch Q_i.

approximation function can be understood as an enrichment function in MFPUM. More examples on different local approximation spaces and its related properties can be found in Refs. [10,23–25].

- *Global approximation function* ${}^{i}N_k$: We denote the approximation function associated with node ${}^{i}n_k$ as ${}^{i}N_k$.

So far we have reviewed the terminologies of MFPUM mainly in one dimension but elements E_i, flat-top region E_i' of partition of unity function ϕ_i, and the support of ϕ_i which is Q_i, can be constructed in two dimension as well. See Fig. 3 for two-dimensional example.

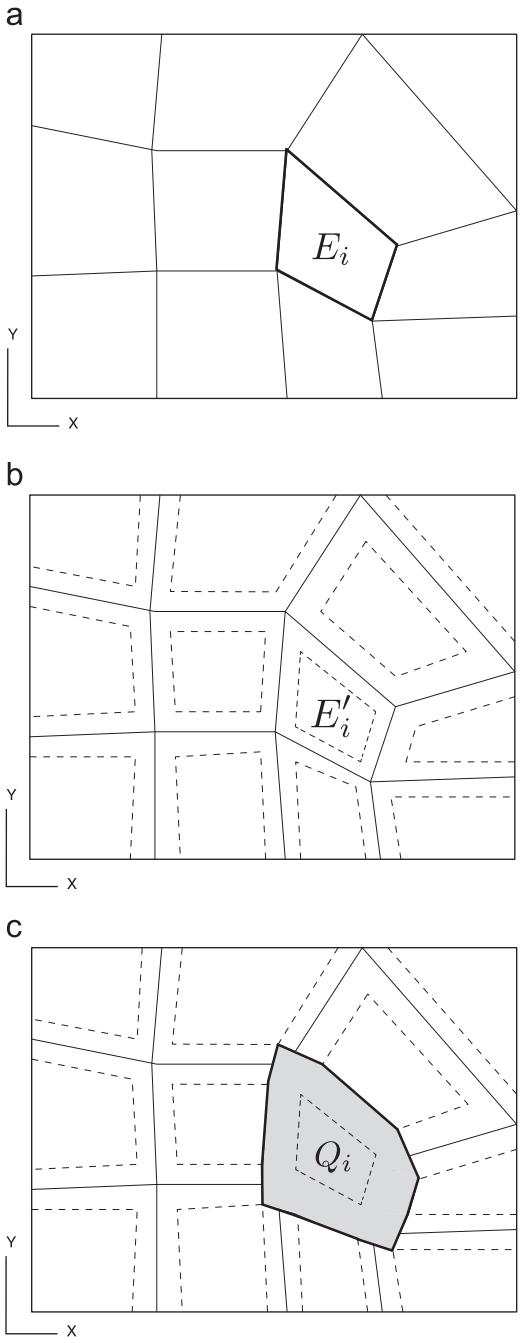

Fig. 3. MFPUM in two dimension: (a) partitioned domain with element E_i; (b) shrunken element E_i' in dotted lines which define flat-top region of PU functions; (c) MFPU patch Q_i.

In a partition of unity method, the approximation $u^{\text{app}}(\mathbf{x})$ is obtained as the sum of the local approximations $u^i(\mathbf{x})$ multiplied by the partition of unity function $\phi_i(\mathbf{x})$ on each patch Q_i as follows:

$$u^{\text{app}}(\mathbf{x}) = \sum_{i=1}^{N} \phi_i(\mathbf{x}) u^i(\mathbf{x}). \tag{2}$$

The linear combination of ${}^{i}L_k$ on ith patch results the local approximation u^i in Eq. (2)

$$u^i(\mathbf{x}) = \sum_{k=1}^{n_i} c_{i_k} {}^{i}L_k(\mathbf{x}), \tag{3}$$

where n_i is the number of nodes distributed on a patch Q_i. Thus, many meshless/meshfree methods including element-free Galerkin method (EFGM) [1], reproducing kernel particle method (RKPM) [2], and method of finite sphere [3] can be viewed as a partition of unity method. However, the partition of unity function ϕ_i that is used for most of meshless/meshfree method is either defined implicitly or in the form of rational functions. In MFPUM, piecewise linear partition of unity function is constructed explicitly with a flat-top feature. A more detailed work including numerical examples can be found in [9].

The higher order polynomial enrichment technique that preserves the Kronecker-delta property was first introduced by Oh et al. [26] in the context of meshless method and adopted by MFPUM. If we substitute $u^i(\mathbf{x})$ in Eq. (2) with Eq. (3) we get the following expression:

$$u^{\text{app}}(\mathbf{x}) = \sum_{i=1}^{N} \sum_{k=1}^{n_i} c_{i_k} (\phi_i(\mathbf{x}) {}^{i}L_k(\mathbf{x})). \tag{4}$$

Therefore, compactly supported global approximation functions ${}^{i}N_k(\mathbf{x})$ are obtained by multiplying flat-top partition of unity function $\phi_i(\mathbf{x})$ with the Lagrange interpolating polynomial ${}^{i}L_k(\mathbf{x})$ as follows:

$${}^{i}N_k(\mathbf{x}) = \phi_i(\mathbf{x}) \cdot {}^{i}L_k(\mathbf{x}), \quad i = 1, \ldots, N; \quad k = 1, \ldots, n_i. \tag{5}$$

An example of second-order ${}^{i}N_k$ in one dimension is shown in Fig. 2(e).

The resulting global approximation function ${}^{i}N_k(\mathbf{x})$ possess the Kronecker-delta property for efficient boundary condition imposition. Using Eq. (5), Eq. (4) can be written as

$$u^{\text{app}}(\mathbf{x}) = \sum_{i=1}^{N} \sum_{k=1}^{n_i} c_{i_k} ({}^{i}N_k(\mathbf{x})). \tag{6}$$

We denote the finite-dimensional vector space spanned by Eq. (5) to be V^{app} and call the Galerkin approximation with the use of the approximation space V^{app} as *mesh based flat-top partition of unity method.*

3. Coupling method

In this section, we first explain how the coupling works in one dimension and then describe how higher order coupling is done in two dimension. The key idea of the coupling is extending the MFPU interpolating function(s) into the transitional area. Some discussions on the coupled system are given at the end of the section.

3.1. Coupling in one dimension

The transitional partition of unity function is a modified mesh based flat-top partition of unity function. The modification is done by augmenting finite element shape function to the flat-top partition of unity function on the transitional area. Let us

illustrate the modification in detail. As shown in Fig. 4(a), we start with partitioned domain with elements. The elements are further categorized to belong one of the subdomains, Ω_C, where finite element method is used, Ω_T where transition occurs, and Ω_F where MFPUM is used. In one-dimensional coupling, exactly one element in Ω_T should suffice to prepare the coupling between MFPUM and FEM. Next, we build flat-top partition of unity functions and interpolating functions on $\Omega_T \cup \Omega_F$ as explained in the previous section, with the help of the supplemental mesh that is shown in Fig. 4(b).

Since there is no overlap between the patch in Ω_T and interfaced finite element in Ω_C, the MFPUM algorithm to create flat-top partition of unity functions in Ω_T fails to satisfy partition of unity in the interfaced region. Let us define the region Q_i' within the patch Q_i where partition of unity is not satisfied as follows:

$$Q_i' = Q_i \backslash \left\{ \mathbf{x} \middle| \sum_{k=1}^{N} \phi_k(\mathbf{x}) = 1 \right\}. \tag{7}$$

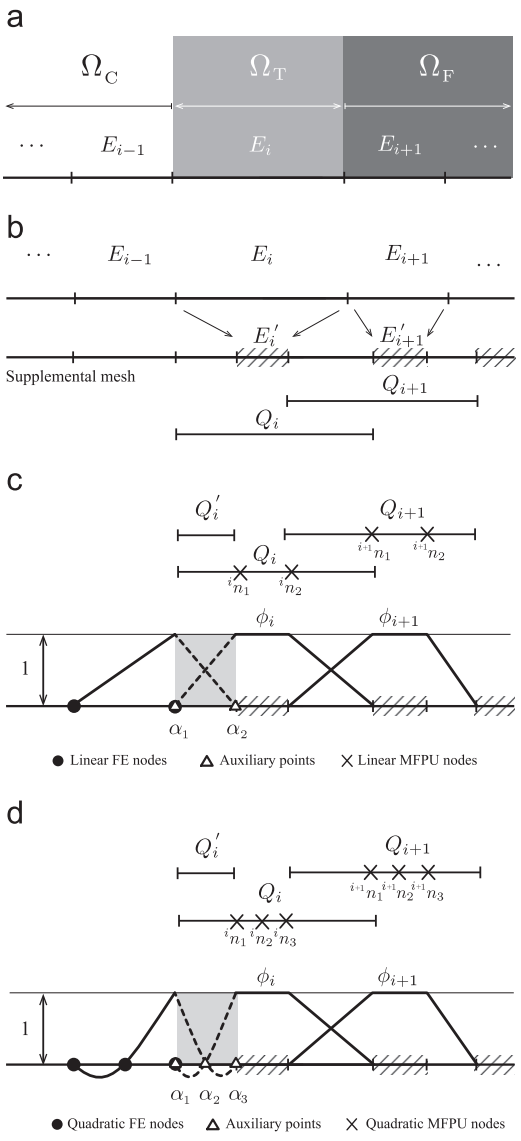

Fig. 4. Coupling in one dimension: (a) partitioned domain with elements; (b) patch construction on Ω_T and Ω_F; (c) linear FE nodal interpolating function and transitional flat-top partition of unity function ϕ_i; (d) quadratic FE nodal interpolating function and transitional flat-top partition of unity function ϕ_i.

It is clear that $Q_i' \neq \emptyset$ for Q_i which belongs to the transitional region. The non-empty intervals Q_i' that is shown in Fig. 4(c) and (d) are such examples in one dimension.

In the case of coupling linear finite element and MFPUM, we place two auxiliary points, α_1 and α_2, on Q_i', see Fig. 4(c) and consider linear finite element shape functions, N_1 and N_2, that correspond to those points. Since point α_1 coincides with one of the existing finite element nodes $\gamma \in \Omega_C$, the shape function N_1 can be assembled to form a nodal interpolating function of γ. The other, N_2, is attached to one of the transitional interpolating functions that interpolates the point α_2. We define the linear transitional function N_τ on the patch Q_i as follows:

$$N_\tau(x) = \begin{cases} \phi_i(x) \cdot {}^{i}L_1(x) & \text{if } x \notin Q_i', \\ N_2(x) & \text{if } x \in Q_i', \end{cases} \tag{8}$$

where $\phi_i(x)$ is the MFPU function given in Eq. (1) and ${}^{i}L_1$ is the linear Lagrange interpolating polynomial defined on the patch Q_i that corresponds to the node ${}^{i}n_1$ defined on E_i'. Thus the transitional interpolating function $N_\tau(x)$ is essentially MFPU interpolating function in $Q_i \backslash Q_i'$ and linear finite element nodal interpolating function in Q_i'. At this point, we can categorize the nodal interpolation functions into N_γ, N_τ, and N_μ by identifying which subdomain includes the nodes associated to the interpolating function. Then the coupled approximation can be written as

$$u^{\text{coupled}} = \sum_{\gamma \in \Omega_C} u_\gamma N_\gamma + \sum_{\tau \in \Omega_T} u_\tau N_\tau + \sum_{\mu \in \Omega_F} u_\mu N_\mu, \tag{9}$$

where u_γ, u_τ, and u_μ are the nodal unknowns.

Proposition 1. *u^{coupled} in Eq. (9) possess polynomial reproducing property of order 1 when linear finite elements are coupled by the transitional function given in Eq. (8).*

Proof. Since each of linear finite element and linear MFPUM has polynomial reproducing property of order 1, we only need to show the polynomial reproducing property in the transitional region Q_i'. For $x \in Q_i'$, u^{coupled} reduces to $u_{\alpha_1} N_\gamma + u_{\alpha_2} N_\tau$ where u_{α_1} and u_{α_2} are two nodal unknowns defined on auxiliary points in Q_i', as shown in Fig. 4(c). Here N_γ and N_τ are nodal interpolating functions corresponding to the nodes α_1 and α_2, respectively. Thus, from Eq. (8), $u_{\alpha_1} N_\gamma + u_{\alpha_2} N_\tau = u_{\alpha_1} N_1 + u_{\alpha_2} N_2$ which is linear interpolation between two nodes u_{α_1} and u_{α_2}. In particular, $u^{\text{coupled}}(x) = \alpha_1 N_1(x) + \alpha_2 N_2(x) = x, \forall x \in Q_i'$. □

Coupling quadratic finite elements with MFPUM is similar to the linear coupling case except there is one extra DOF involved. We use three additional finite element shape functions on Q_i', the grayed interval (α_1, α_3) in Fig. 4(d). Note that $\gamma \in \Omega_C$ coincides with auxiliary point α_1. Among the three finite element shape functions, N_1, N_2, and N_3, that corresponds to the auxiliary points α_1, α_2 and α_3, we assemble N_1 to the existing finite element nodal interpolating function N_γ. The bubble function N_2 is responsible to the extra DOF. N_3 is augmented to the quadratic transitional interpolating functions N_τ on the patch Q_i that interpolates the point α_3 as follows:

$$N_\tau(x) = \begin{cases} \phi_i(x) \cdot {}^{i}L_1(x) & \text{if } x \notin Q_i', \\ N_3(x) & \text{if } x \in Q_i', \end{cases} \tag{10}$$

where $\phi_i(x)$ is the MFPU function in Eq. (1) and ${}^{i}L_1$ is the quadratic Lagrange interpolating polynomial defined on the patch Q_i which corresponds to the node ${}^{i}n_1$. The auxiliary functions N_1 and N_3 are shown in dotted line in Fig. 4(d). With quadratic transitional function N_τ in Eq. (10), we establish the following proposition.

Proposition 2. *u^{coupled} in Eq. (9) possess polynomial reproducing property of order 2 when quadratic finite elements are coupled by the quadratic transitional function given in Eq. (10).*

Proof. Following the argument in the proof of Proposition 1, we only need to show the polynomial reproducing property in the transitional region Q_i'. For $x \in Q_i'$, u^{coupled} reduces to $u_{\alpha_1}N_\gamma + u_{\alpha_2}N_2 + u_{\alpha_3}N_\tau$ where u_{α_1}, u_{α_2}, and u_{α_3} are nodal unknowns defined on the three auxiliary points, as shown in Fig. 4(d). Restricted on Q_i', N_γ and N_τ are quadratic finite element nodal interpolating functions corresponding to the nodes α_1 and α_3, respectively. Thus, from Eq. (10), $u_{\alpha_1}N_\gamma + u_{\alpha_2}N_2 + u_{\alpha_3}N_\tau = u_{\alpha_1}N_1 + u_{\alpha_2}N_2 + u_{\alpha_3}N_3$ which results quadratic interpolation of three nodes u_{α_1}, u_{α_2} and u_{α_3}. More specifically, $u^{\text{coupled}}(x) = (\alpha_1)^2N_1(x) + (\alpha_2)^2N_2(x) + (\alpha_3)^2 N_3(x) = x^2$, $\forall x \in Q_i'$. □

The simple and effective idea for coupling finite elements and MFPUM in one dimension can be extended to two dimension.

3.2. Coupling in two dimension

Converting a single element to a patch was enough for one dimensional coupling. On the contrary, in two dimension, the transitional patch may contain more than one subpatches. Let us illustrate the coupling procedure with an example. Fig. 5(a) shows the decomposed domain and Fig. 5(b) shows two patches defined by the supplemental mesh. Q_i' is defined in Eq. (7). $Q_1' = e_1 \cup e_2$, $Q_4' = e_2 \cup e_3$ and $Q_1' \cup Q_4' = e_1 \cup e_2 \cup e_3$ as shown in Fig. 5(c). $Q_1' \cup Q_4'$ represents the region where auxiliary finite element shape functions will be created for coupling. To create auxiliary shape functions, we populate necessary auxiliary points in each subpatches, e_1, e_2, and e_3. Fig. 5(c) and (d) shows auxiliary points on the subpatches e_1,e_2, and e_3 that is required for linear coupling and quadratic coupling, respectively. Note that the order of auxiliary function will be one order higher in the normal direction of the interfaced finite element edge. Similar to what we have done in one dimension, auxiliary shape functions will be either assembled to existing finite element nodal interpolating function if the auxiliary point coincides with existing finite element node or used to augment MFPU interpolating function if the auxiliary point coincides with existing MFPU node. If the auxiliary point is not a hanging node and neither coincides with the existing finite element node nor the existing MFPU node, the corresponding shape function will be used independently and will result an extra DOFs in the coupled system.

Unlike in one dimensional coupling, some of the auxiliary points end up hanging nodes. The hanging node has a special purpose in two-dimensional coupling. It is to raise the polynomial order on the side, for example, the common edge of e_2 and e_4 of Fig. 5(c). The MFPU interpolating function has one higher polynomial order in the non flat-top area, for example e_4. Augmenting the auxiliary finite element shape function that is defined on e_2 to the MFPU interpolating function, we have to introduce shape functions that have one order higher than the local approximation functions of MFPU patch in the non flat-top area e_4. In the following, we will define the transitional interpolating function on a transitional patch Q_i

$$N^i_{\tau,\,k}(x,y) = \begin{cases} F(x,y) = \phi_i(x,y)^i L_k(x,y) & \text{if } (x,y) \notin Q_i', \\ N_{\mathcal{A},k}(x,y) & \text{if } (x,y) \in \mathcal{A} = Q_i' \setminus \bigcup_{\substack{j=1 \\ j \neq i}}^{N} Q_j', \\ N_{\mathcal{B},k}(x,y) + \sum_j F(x_{h_j}, y_{h_j}) N_{\mathcal{B},h_j}(x,y) & \text{if } (x,y) \in \mathcal{B} = \bigcup_{\substack{j=1 \\ j \neq i}}^{N} (Q_i' \cap Q_j'), \end{cases} \tag{11}$$

where $N_{\mathcal{A},k}$ is one of the finite element shape function defined on $\mathcal{A}$ which has the auxiliary point coincides with the MFPU node k, $N_{\mathcal{B},k}$ is one of the finite element shape function defined on $\mathcal{B}$ which has the auxiliary point coincides with the MFPU node k,

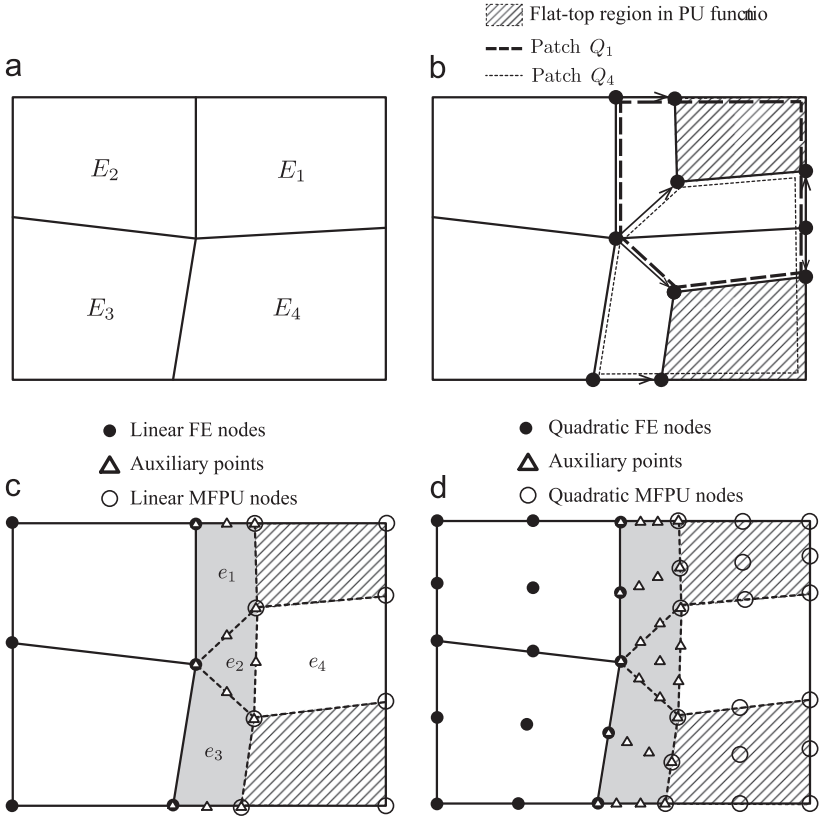

Fig. 5. Two-dimensional coupling preparation: (a) partitioned domain with four elements; (b) construction of two transitional patches; nodes and auxiliary points distribution in two dimension for (c) linear coupling and (d) quadratic coupling.

and (x_{h_j}, y_{h_j}) are the location of j's hanging node and $N_{\mathcal{B},h_j}$ is the corresponding auxiliary shape function defined on $\mathcal{B}$. For the patch Q_1 shown in Fig. 5, $\mathcal{A}=e_1$ and $\mathcal{B}=e_2$. Also for the patch Q_2 in Fig. 5, $\mathcal{A}=e_3$ and $\mathcal{B}=e_2$.

Proposition 3. *u^{coupled} in Eq. (9) possess polynomial reproducing property of order k when order k finite elements are coupled by the transitional function given in Eq. (11).*

Proof. We only need to show the polynomial reproducing property in the transitional region Q_i'. Restricted on $\mathcal{A}$, we only have finite element shape functions left which clearly interpolates polynomials up to degree k. Hence, the result is clear. On the other hand, when restricted on $\mathcal{B}$, u^{coupled} in Eq. (9) has only finite element shape functions including the following shape function which is the interpolation function associated with the hanging node j

$$\sum_i\sum_k F(x_{h_j},y_{h_j})N_{\mathcal{B},h_j}(x,y)=\sum_i\sum_k \phi_i(x_{h_j},y_{h_j})^{\mathrm{i}}L_k(x_{h_j},y_{h_j})N_{\mathcal{B},h_j}(x,y) \tag{12}$$

$$\sum_i\sum_k F(x_{h_j},y_{h_j})N_{\mathcal{B},h_j}(x,y)=\sum_i \phi_i(x_{h_j},y_{h_j})N_{\mathcal{B},h_j}(x,y)\sum_k{}^{\mathrm{i}}L_k(x_{h_j},y_{h_j}) \tag{13}$$

$$\sum_i\sum_k F(x_{h_j},y_{h_j})N_{\mathcal{B},h_j}(x,y)=\sum_i \phi_i(x_{h_j},y_{h_j})N_{\mathcal{B},h_j}(x,y)\times 1 \tag{14}$$

$$\sum_i\sum_k F(x_{h_j},y_{h_j})N_{\mathcal{B},h_j}(x,y)=N_{\mathcal{B},h_j}(x,y)\sum_i \phi_i(x_{h_j},y_{h_j}) \tag{15}$$

$$\sum_i\sum_k F(x_{h_j},y_{h_j})N_{\mathcal{B},h_j}(x,y)=N_{\mathcal{B},h_j}(x,y)\times 1 \tag{16}$$

$$\sum_i\sum_k F(x_{h_j},y_{h_j})N_{\mathcal{B},h_j}(x,y)=N_{\mathcal{B},h_j}(x,y). \tag{17}$$

Therefore, as in the case of restricted on $\mathcal{A}$, in the restricted region $\mathcal{B}$, all we have in the region $\mathcal{B}$ is auxiliary finite element shape functions which can interpolate order k polynomials. □

3.3. Coupled system

Let us consider the following variational problem on a bounded polygonal domain Ω: Find $u\in H^1(\Omega)$ such that $u=u_d$ on Γ_D and

$$a(u,v)=f(v) \text{ for all } v\in H_0^1(\Omega). \tag{18}$$

For the Poisson equation, $a(u,v)$ and $f(v)$ are given as follows:

$$a(u,v)=\int \nabla u\cdot\nabla v\, d\Omega, \tag{19}$$

$$f(v)=\int fv\, d\Omega+\int v\nabla u\cdot\hat{\mathbf{n}}\, d\Gamma, \tag{20}$$

where $\hat{\mathbf{n}}$ is the outward normal vector along boundary Γ.

In the case of two-dimensional linear elasticity, the equilibrium equations are given in terms of displacement vector $\mathbf{u}=\{u_x,u_y\}$ as follows:

$$\mathbf{D}^{\mathrm{T}}\,\mathbf{E}\,\mathbf{D}\,\mathbf{u}(\mathbf{x})+\mathbf{f}(\mathbf{x})=\mathbf{0}, \tag{21}$$

subjected to the boundary conditions,

$$\mathbf{N}\,\mathbf{D}\,\mathbf{u}(\mathbf{s})=\tilde{\mathbf{T}}(\mathbf{s}),\quad \mathbf{s}\in\Gamma_{\mathrm{T}}, \tag{22}$$

$$\mathbf{u}(\mathbf{s})=\tilde{\mathbf{u}}(\mathbf{s}),\quad \mathbf{s}\in\Gamma_{\mathrm{D}}, \tag{23}$$

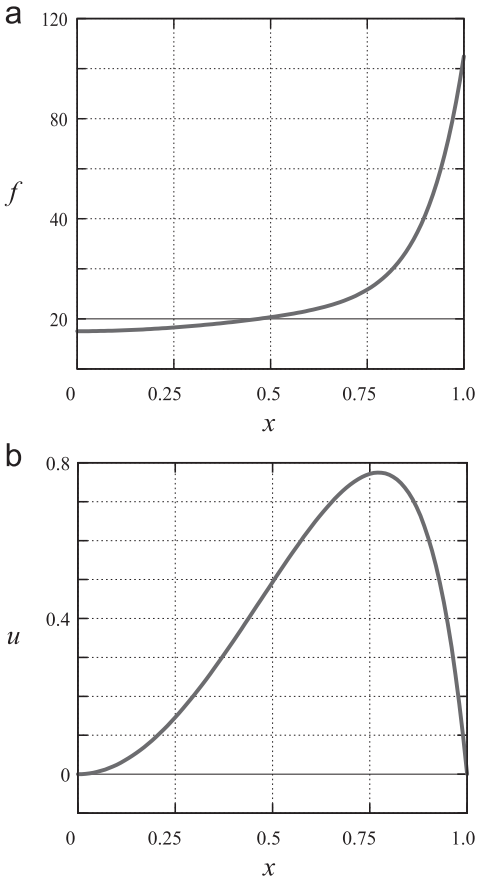

Fig. 6. A one-dimensional heat conduction problem: (a) distributed heat source of intensity f; (b) temperature distribution u.

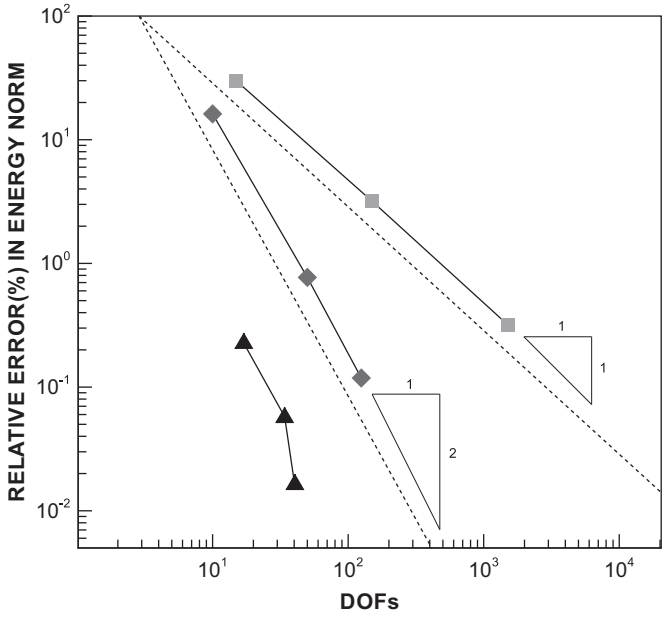

Fig. 7. Convergence rate comparison between coupled formulations for the heat conduction model: squares represent the convergence of linear coupling, diamonds represent the convergence of quadratic coupling, and triangles represent the convergence of quadratic finite elements coupled with a single MFPUM that has order eight.

where $\Gamma_T \cup \Gamma_D = \partial\Omega$

$$\mathbf{D} = \begin{bmatrix} \frac{\partial}{\partial x} & 0 & \frac{\partial}{\partial y} \\ 0 & \frac{\partial}{\partial y} & \frac{\partial}{\partial x} \end{bmatrix}^T, \quad \mathbf{N} = \begin{bmatrix} n_x & 0 & n_y \\ 0 & n_y & n_x \end{bmatrix}, \quad \mathbf{E} = E_{ij},\ 1 \le i,\ j \le 3$$

is the symmetric positive definite material constant matrix.

The variational problem corresponding to Eq. (21) is to find the vector $\mathbf{u} = \{u_x, u_y\}$ such that $u_x,\ u_y \in H^1(\Omega), \mathbf{u} = \tilde{\mathbf{u}}$ on Γ_D and

$$a(\mathbf{u},\mathbf{v}) = \mathbf{f}(\mathbf{v}) \quad \text{for all } \mathbf{v} \in H_0^1(\Omega). \tag{24}$$

The bilinear form $a(\mathbf{u},\mathbf{v})$ and $f(\mathbf{v})$ are given as follows:

$$a(\mathbf{u},\mathbf{v}) = \int_\Omega (\mathbf{D}\,\mathbf{v})^T\,\mathbf{E}(\mathbf{D}\mathbf{u})\,dx\,dy, \tag{25}$$

$$\mathbf{f}(\mathbf{v}) = \int_\Omega \mathbf{v}^T\mathbf{f}\,dx\,dy + \int_{\Gamma_T} \mathbf{v}^T\tilde{\mathbf{T}}\,ds, \tag{26}$$

where $\mathbf{f}$ is the vector of the body force per unit area, and $\tilde{\mathbf{T}}$ is the traction vector.

4. Numerical examples

The coupling between the FEM and MFPUM is mutually beneficial; coupling enables enrichment to higher order FEM and makes MFPUM more economical by saving DOFs. We highlight two important features of our proposed coupling:

Feature (1) Flexible enriched area: The enriched zone can be widened or shrunken on a fixed mesh. In other words,

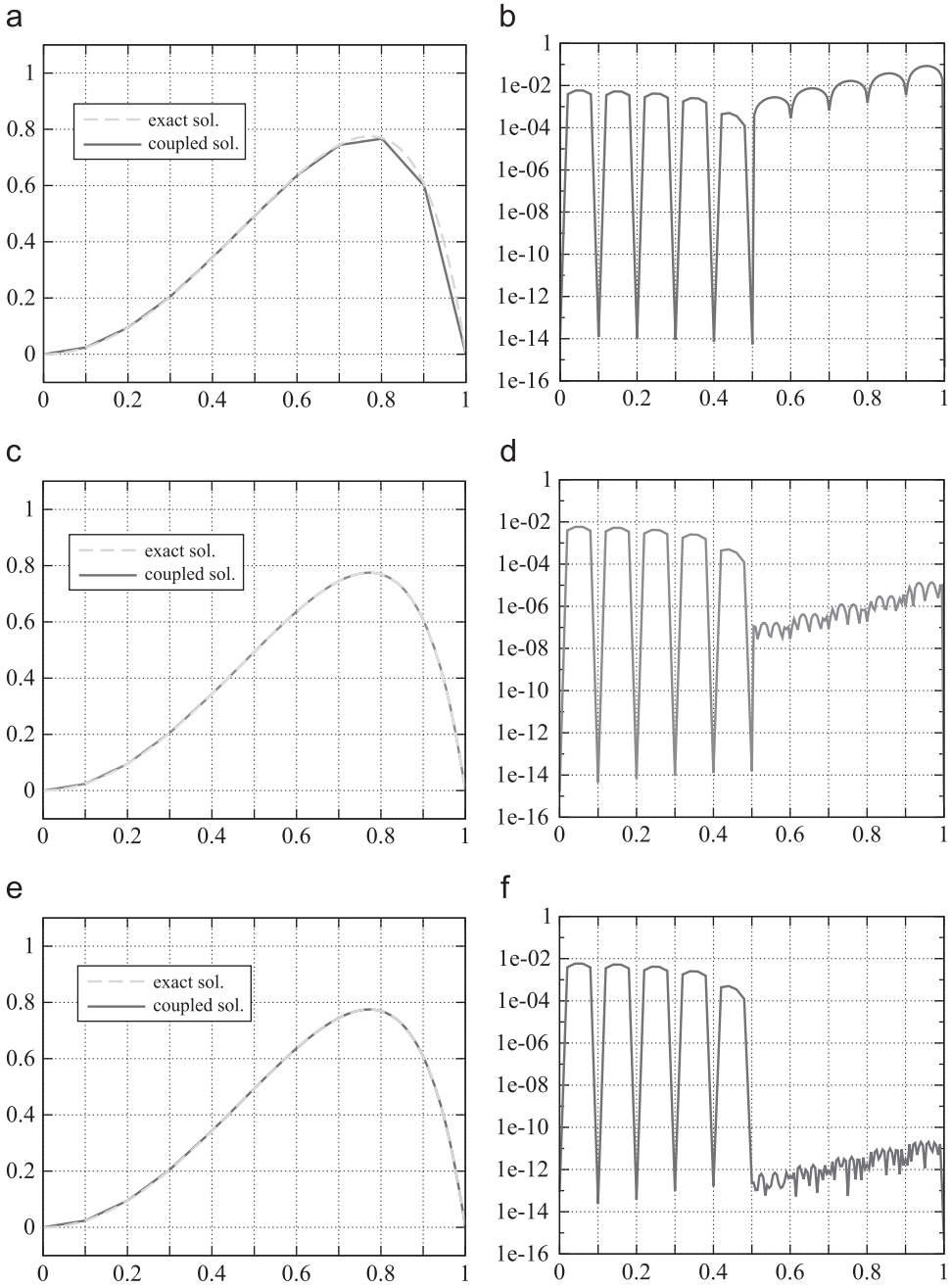

Fig. 8. Comparison between exact solution and coupled approximation of: five linear finite elements coupled with five (a) first-order MFPUM and its error plot (b); (c) fourth-order MFPUM and its error plot (d); (e) eighth-order MFPUM and its error plot (f).

we can transfer finite elements to flat-top partition unity patches and vise versa.

Feature (2) Consistent polynomial reproducing order: The polynomial enrichment order of MFPUM can be matched to the order of the finite element that is interfaced to obtain consistent polynomial reproducing property.

The polynomial reproducing property, Feature (2), allows the coupled approximation to interpolate not only a constant field but also a linear field on entire computational domain. This is important when an elasticity problem is considered with a displacement-based formulation because constant fields and linear fields represent rigid body modes and constant strain states, respectively.

In this section, we demonstrate three examples with the proposed coupling method. We will denote $\|e\|_E$ as the relative error in the energy norm and $\|e\|_E(\%)$ as the relative error in energy norm in percent which is $\|e\|_E \times 100$. Throughout this section unless it is noted separately we have used fixed flat-top parameter $\chi = 0.95$ for mesh based flat-top partition of unity method (MFPUM).

4.1. A heat conduction problem on a bar with a boundary layer

To test the coupled formulation, a heat conduction problem temperature fixed to be zero at the end points in one dimension is considered. Let us denote the heat flow in a heat conducting bar as q, the heat conductivity as k, and the distributed heat source of intensity as f. Then under the assumption that the heat flow in a heat conducting bar follows the Fourier's law $-q = ku'$ with $k=1$ along with the energy conservation $q' = f$ can model the temperature distribution on the bar by the following Poisson equation:

$$-u''(x) = f(x) \quad x \in (-1,1), \quad u(-1) = u(1) = 0. \tag{27}$$

The analytic solution of Eq. (27) with the heat source $f(x) = -0.5\pi^2 \cos(\pi x) + 100 \cosh(10x)/\cosh(10)$ is $u(x) = -\cosh(10x)/\cosh(10) + \cos^2(0.5\pi(x+1))$ which can be easily verified by direct substitution. The heat source $f(x)$ and analytic temperature distribution $u(x)$ is shown in Fig. 6(a) and (b), respectively.

The coupling is targeted to capture the boundary layer that is presented near $x=1$. We apply the coupling method on a uniformly spaced mesh with finite element method on the left half of the given interval, (0,0.5), and MFPUM on the right half of the interval, (0.5,1).

The consistency of the coupled approximation is tested. When linear finite elements are coupled with first-order MFPU patches, the coupled approximation should be able to reproduce polynomial of

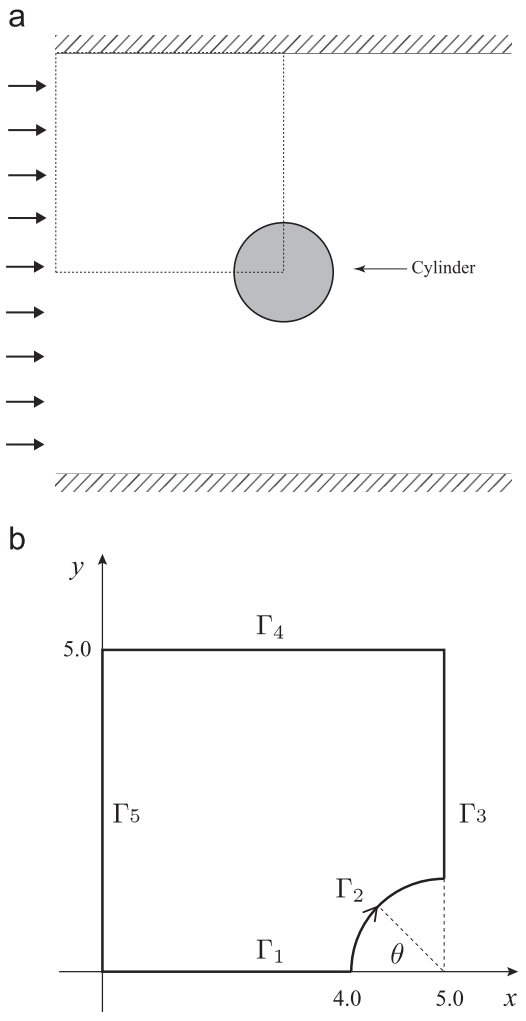

Fig. 9. A cylinder placed in an inviscid flow: (a) quarter of the flow region is outlined; (b) configurations for the quarter model.

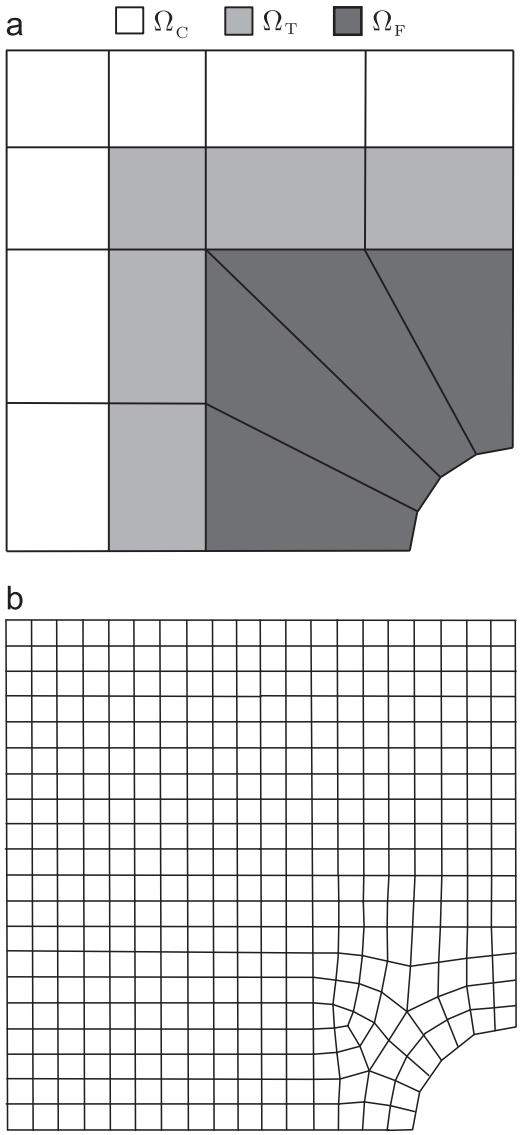

Fig. 10. Mesh preparation: (a) coarse mesh with 16 elements for the coupled formulation; (b) finer mesh with 383 elements and 455 nodes for finite element approximation.

order one on the entire computational domain. Likewise, polynomial reproducing of order two is expected for quadratic finite elements coupled with second-order MFPU patches. When the solution is smooth ($u \in C^{\infty}$), like in this example, we expect the error in energy norm of coupled approximation to show the rate of convergence $O(h)$ in linear coupling case and $O(h^2)$ in quadratic coupling case, where h indicates the element size.

In one dimension $h \sim 1/N$; thus we have plotted the relative error in energy norm versus degrees of freedom to test the coupled convergence, see Fig. 7. The coupled approximation has same h size for finite elements and MFPU patches. The coupled approximation showed similar performance compared to finite element approximation applied on entire computational domain when the order of MFPUM is matched with the order of finite element method. The expected rate of convergence in energy norm agrees well with the expected convergence rate as shown in Fig. 7. On the other hand, we can increase the rate of convergence by increasing only the order on MFPU patches. The filled triangles in Fig. 7 demonstrate such improvement in convergence. They are obtained by uniformly refined finite elements in (0,0.5) coupled with a single MFPU patch in (0.5,1) that has order eighth.

In this example, the boundary layer is located near $x=1$. The high-order partition of unity enrichment is especially well suited for capturing such behavior. Fig. 8(a)–(f) shows the effectiveness of the high-order polynomial enrichment to deal with the boundary layer.

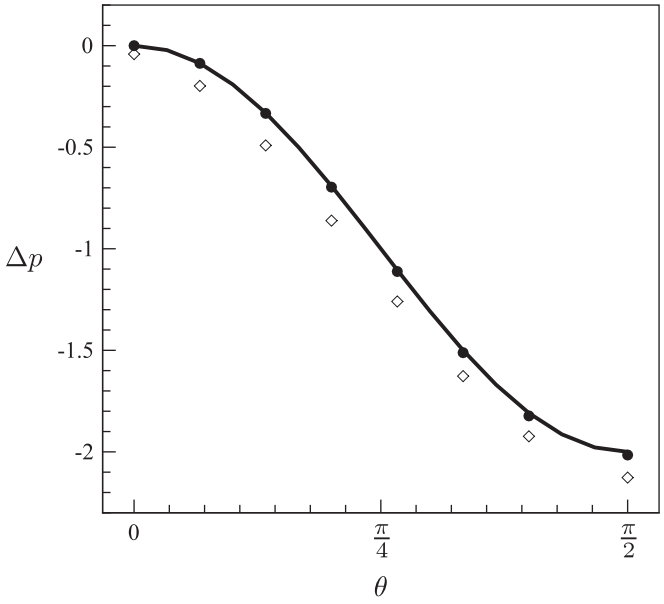

Fig. 12. The pressure difference $\Delta p = p - p_s$ on the surface of the cylinder. Solid line is the pressure from potential theory. Filled dots are the pressure obtained by coupled approximation, and diamonds are the approximated pressure by linear finite elements.

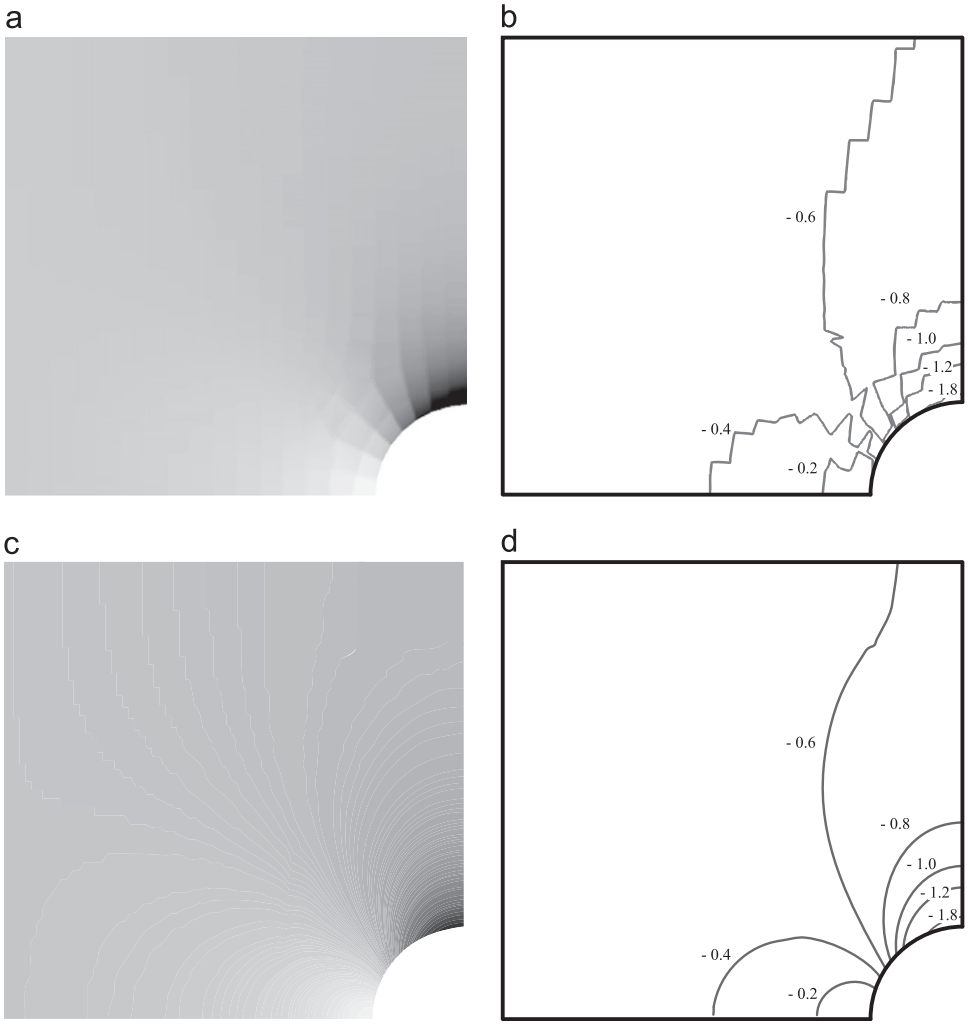

Fig. 11. Pressure plot and its corresponding contours: (a) and (b) are obtained by coupled approximation; (c) and (d) are obtained by linear finite element approximation.

We see that the error in Ω_F quickly decreases as we increase the enrichment order.

4.2. Potential flow around a cylinder

Next we simulate a potential flow of an inviscid fluid around a cylinder, as shown in Fig. 9(a). We approximate the velocity potential u by solving the Laplace equation $\Delta u = 0$ on the rectangular domain with a circular hole. Because of the symmetry, we only consider a quarter portion of the model, see Fig. 9(b). We denote normal vector to the surface $\hat{\mathbf{n}}$. The boundary conditions on Γ_i, $i = 1, \ldots, 5$ for the quarter model is given as follows:

(i) The boundary condition on Γ_1, Γ_2 and Γ_4 is set to $\nabla u \cdot \hat{\mathbf{n}} = 0$. The boundary condition on Γ_1 is to enforce the symmetry of the quarter model. The boundary condition on Γ_2 and Γ_4 follows from the no penetration condition on the wall.
(ii) On anti-symmetric line Γ_3, we set $u=0$. It is clear that imposing Neumann condition on Γ_3 is impossible because the profile of the flux is not known for the quarter model. Mathematically, assigning a arbitrary constant will suffice because the velocity along Γ_3 is independent of the constant value that is chosen.
(iii) The inlet boundary condition on Γ_5 is taken from the full model and has to be Neumann type. We assign $\nabla u \cdot \hat{\mathbf{n}} = -1$ on Γ_5. In other words, a uniform flow of speed 1 is assumed on the inlet.

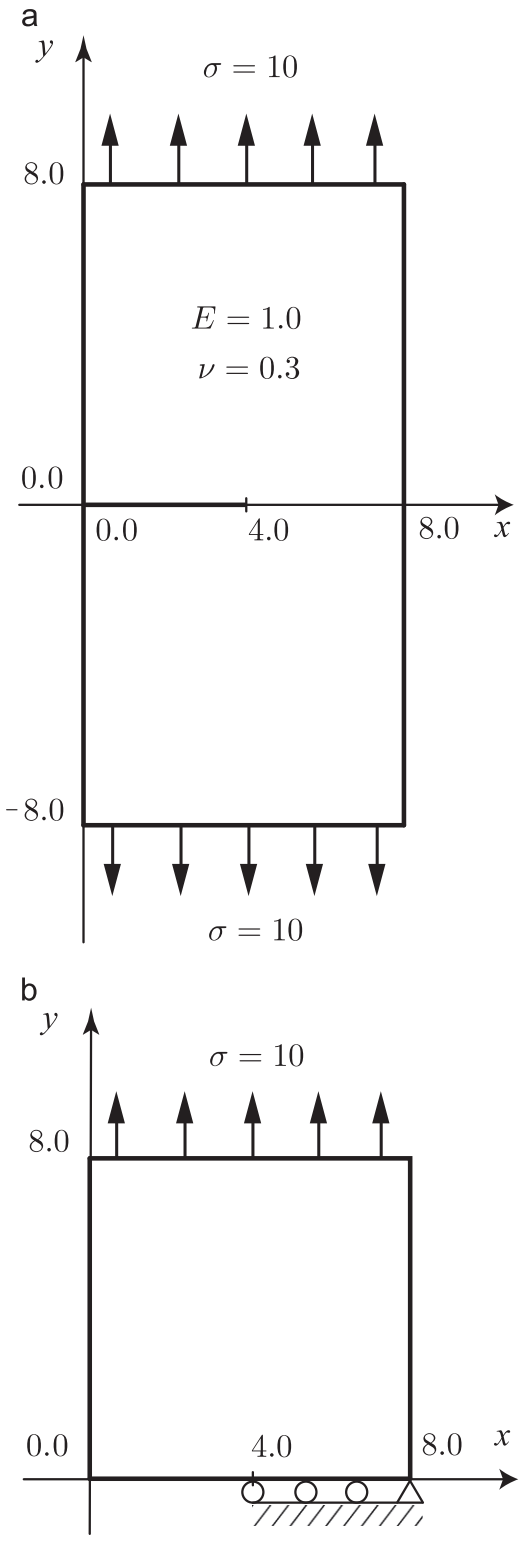

Fig. 13. Single edge cracked plate under uniform tension: (a) full model; (b) half model.

The following observations suggest a coupling scheme shown in Fig. 10(a). First, we expect a nearly uniform flow pattern away from the cylinder. Hence, the velocity potential away from the cylinder will be well approximated with lower order finite elements. Second, the speed of the flow will decrease in front of the cylinder and increase at the side of the cylinder due to the pressure difference. Also, the pressure drop around cylinder should be smooth; therefore, higher order approximation would be more appropriate. Thus, we placed four fourth-order enriched MFPU patches around the cylinder surface to capture the smooth drop of the pressure.

The coupled numerical approximation is validated by comparing known analytic pressure on the surface of cylinder obtained by potential theory. At the surface of the cylinder, the known velocity potential along with Bernoulli's principle results $p_s = p + 2\rho U^2 \sin^2\theta$, where ρ is the density, U is the free-stream velocity far away from the cylinder, and p_s is the stagnation pressure. In this example, we have $\rho = 1$ and $U = 1$. The pressure relative to the stagnation pressure is, therefore, $\Delta p = p - p_s = 2\sin^2\theta$. On the other hand, the pressure presented in Fig. 11 is calculated using the computed ∇u and Bernoulli's principle, $p = -\frac{1}{2}|\nabla u|^2$. Since, the pressure

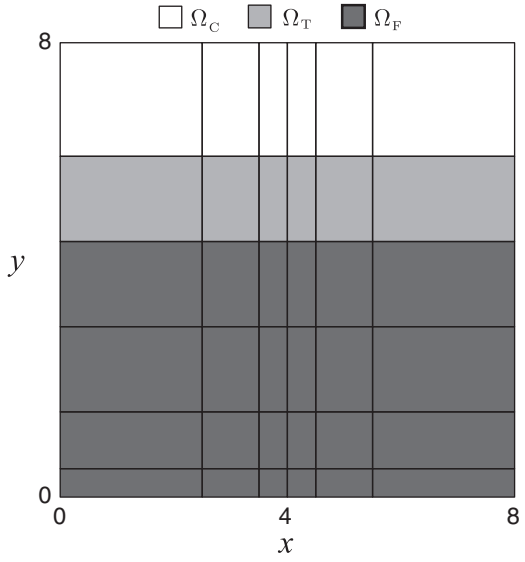

Fig. 14. Mesh used for coupled approximation on a half modeled single edge cracked plate.

calculation involves derivative of the velocity potential, the linear finite element approximation, which has constant gradient within elements, shows clear inter-element jump in the pressure as shown in Fig. 11(a) and (b). Coupled approximation, however, shows smoother pressure compared to linear finite element approximation because the ∇u is approximated by higher order polynomials. See Fig. 11(c) and (d).

The approximations for the pressure are further compared on the surface of the cylinder where the relative pressure to the stagnation pressure is known. As shown in Fig. 12, the coupled approximation is in a good agreement with the pressure obtained by potential theory and performs better than linear finite elements with more DOFs. The finite element approximation with the mesh shown in Fig. 10 has more than 50% of DOFs compared to the coupled approximation near the surface of the cylinder. The advantage of coupling with higher order interpolation on the region of interest is clearly shown.

4.3. A single-edge cracked plate under uniform tension

In this example, we apply the coupling technique to a linear elasticity problem on an edge cracked domain. A rectangular domain $\Omega = \{(x,y) : 0 \le x \le 8, -8 \le y \le 8\}$ with a crack of length 4 along the x-axis is considered. Young's modulus $E = 1$, Poisson's ratio $\nu = 0.3$, and plane stress condition is assumed. To enforce opening mode only, a uniform tension $\chi = 10$ is applied in the y-direction. The geometry description and material constants are given in Fig. 13(a). Because of the symmetry we only use half model for actual computation. The half model is shown in Fig. 13(b) with additional boundary condition on the axis of symmetry. The y-displacement is fixed along the x-axis excluding

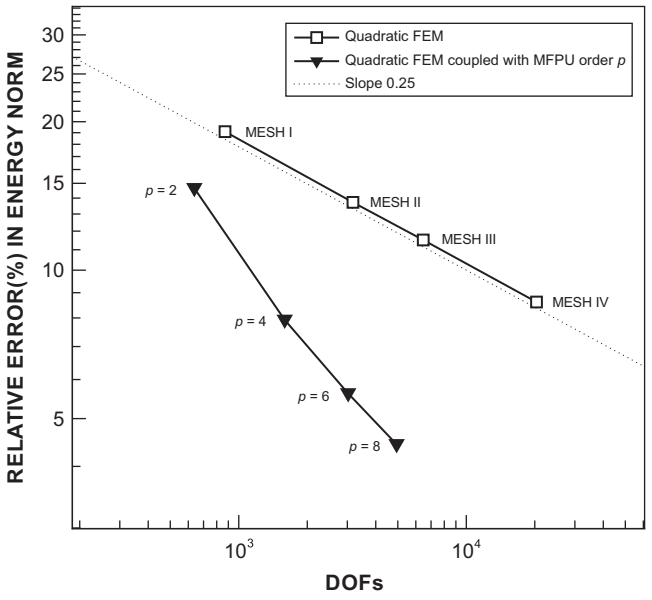

Fig. 16. Convergence comparison between quadratic finite element approximation and coupled approximation in strain energy.

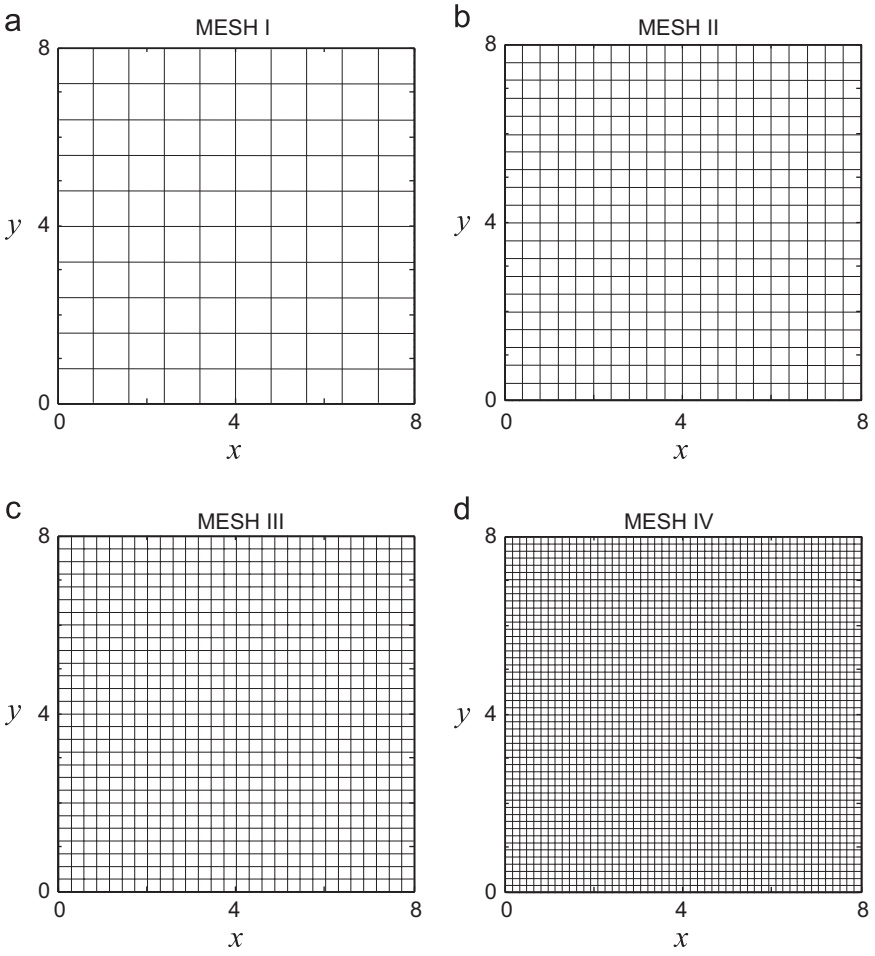

Fig. 15. Mesh sequence for quadratic finite element approximation: (a) MESH I—100 elements (10×10); (b) MESH II—400 elements (20×20); (c) MESH III—784 elements (28×28); (d) MESH IV—2500 elements (50×50).

the crack surface, and the bottom right corner is fully clamped to prevent rigid body motion.

We have used the displacement based weak formulation, Eq. (24) for all the computation in this example. We expect that the displacement field, which is our primary variable for the approximation, will be smooth enough away from the crack tip. Hence, we place quadratic finite elements away from the crack tip and use MFPUM with higher order polynomial enrichment around crack-tip. Fig. 14 shows the mesh and coupling scheme. Fig. 15 shows the mesh sequence that will be used for quadratic finite element approximations. Note that the coupled approximation uses relatively coarse mesh and it is designed to have more DOFs around the crack-tip compared to uniformly graded mesh. On Ω_F and Ω_T, we have used the flat-top parameter $\chi = 0.99$ to construct partition of unity patches and quadratic finite elements are coupled with quadratic transitional functions.

The coupled approximation and finite element approximation are benchmarked with the result of Beckers et al. [27]. They used dual analysis and Richardson's extrapolation with very fine meshes to estimate exact strain energy of this example problem to be 8085.7610. The results are summarized in the graph, see Fig. 16 for the convergence of strain energy in energy norm.

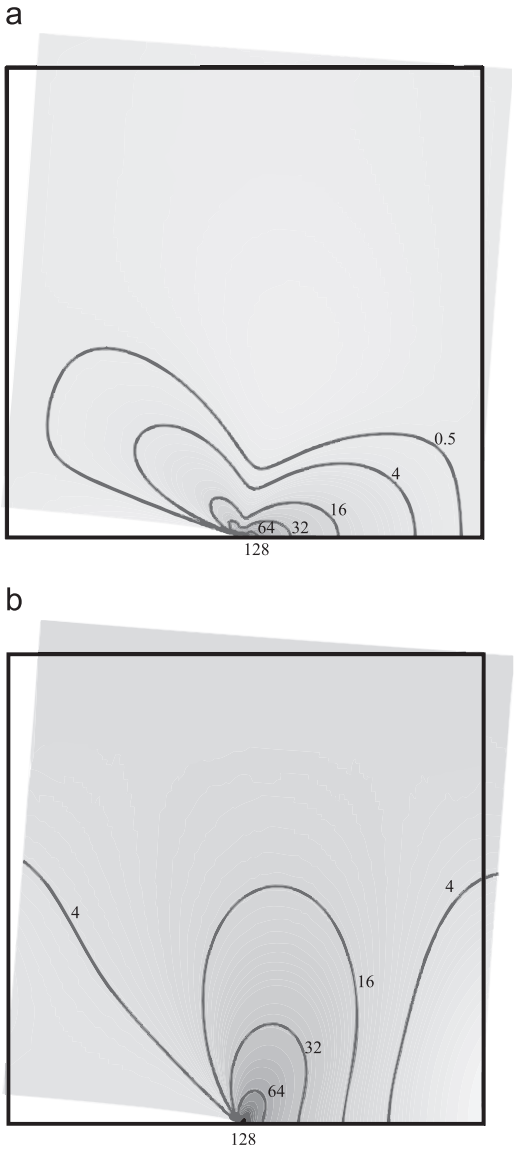

Fig. 17. Stresses on the deformed body obtained by coupled approximation: (a) σ_{xx} and (b) σ_{yy}.

Table 1
Stress intensity factor obtained by coupled approximation.

Δa	p	SIF	*Rel. err* (%)
10^{-3}	2	96.45	(3.75)
	4	98.96	(1.25)
	6	99.53	(0.68)
	8	99.78	(0.43)
10^{-4}	2	96.45	(3.75)
	4	99.21	(1.00)
	6	99.75	(0.46)
	8	100.55	(0.23)
Reference		100.21	

We see that coupled approximation, which has fewer DOFs, gives a better estimate for the strain energy calculation than quadratic finite element calculation. With higher order enrichment $p=8$ on a relatively coarse mesh, the relative error in energy norm is less than 5% which is accurate enough to be used in engineering decision. We present the computed stress component σ_{xx} and σ_{yy} on a deformed shape of the body, see Fig. 17.

The meshes we have used for this example are chosen for clear demonstration and convenience not for optimized performance. Also, the size and location of enrichment are determined by physical intuition rather than utilizing an error indicator. Therefore, it is unlikely that the setup we have used for our coupling is an optimal choice. We could have dealt with the singularity by using exponentially graded mesh toward the point of singularity or enriching the flat-top partition of unity patch with non-polynomial singular functions as it is normally done in GFEM or XFEM. Nevertheless, we have not incorporated these options to our presentation because the coupled solution with higher order polynomials already resulted accurate solution.

We further validate the effectiveness and accuracy of coupled approximation by estimating the stress intensity factor for this example problem. For the single edge cracked plate under uniform tension, the mode I stress intensity factor can be obtained as follows [28]:

$$K_I = \sigma\sqrt{\pi a}\left[1.12-0.23\left(\frac{a}{b}\right)+10.55\left(\frac{a}{b}\right)^2-21.72\left(\frac{a}{b}\right)^3+30.39\left(\frac{a}{b}\right)^4\right], \quad \left(\frac{a}{b}\right) < 0.6, \tag{28}$$

where a is the crack length and b is the width of the plate. Using Eq. (28), we get the reference stress intensity factor $K_I = 100.21$ for our example problem. There are several techniques to calculate the stress intensity factor; crack extension, stiffness derivative, and J-integral to name but a few. In this example, the crack extension technique is used. When the crack extends by amount Δa, the strain energy will relax. In other words, extension of crack causes a decrease of the stored energy which we denote by ΔU. The decrease in stored energy is known as the strain energy release rate, G,

$$G = -\frac{\Delta U}{\Delta a} = -\frac{U_2 - U_1}{a_2 - a_1}. \tag{29}$$

The stress intensity factor K_I for the plane stress case is related to the energy release rate **G** as follows:

$$K_I = \sqrt{EG}, \tag{30}$$

where E is Young's modulus. The stress intensity factor computed by Eq. (30) corresponds to the crack length $(a_1+a_2)/2$.

To estimate the mode I stress intensity factor by the crack extension, we calculate the change in strain energy (ΔU) by

extending the crack length Δa by 10^{-3} and 10^{-4}. The computed stress intensity factors by coupled approximation with different enrichment orders p is summarized in Table 1. With the increase of p, the stress intensity factor converges to the reference value within 1% of relative error.

5. Concluding remarks

A seamless coupling between finite elements with mesh based flat-top partition of unity method is developed and tested on simple one- and two-dimensional problems. The same approach is applicable to three dimensions and also for the plate and shell analyses [29–31] and cohesive cracks [32–34]. The proposed coupling method clearly showed the effectiveness of coupling finite element method with mesh-based flat-top partition of unity method. For those examples that we have considered, the coupled formulation, which has significantly fewer DOFs, not only outperformed the finite element method but also showed the potential use to deal with boundary layers and singularities. On the other hand, the method of auxiliary mapping (MAM), which is known as a technique that is built right into the p-version of finite element method, is highly effective to capture some singularities, such as crack singularity in elasticity problems [35]. However, the partition of unity enrichment technique can virtually deal any known singularities, and can be applied to those problems that MAM may fail. Although we have not explored the option in this paper, we expect the coupling with the singular enrichment could improve the result of the cracked problem we have presented significantly and also applicable to those problems that MAM shows difficulty. We would like to deal this issue in future study.

Acknowledgments

This work was supported by the Human Resources Development (No. 20114030200040) of the Korea Institute of Energy Technology Evaluation and Planning (KETEP) grant funded by the Korea Government Ministry of Knowledge Economy. The current paper is greatly improved under suggestions from anonymous referees. We are grateful for their efforts in helping us reshape the writing.

References

[1] T. Belytschko, Y.Y. Lu, L. Gu, Element-free Galerkin methods, Int. J. Numer. Methods Eng. 37 (2) (1994) 229–256.
[2] W.K. Liu, S. Jun, Y.F. Zhang, Reproducing kernel particle methods, Int. J. Numer. Methods Fluids 20 (8–9) (1995) 1081–1106.
[3] S. De, K.J. Bathe, The method of finite spheres, Comput. Mech. 25 (4) (2000) 329–345.
[4] H.S. Oh, J.G. Kim, J.W. Jeong, The closed form reproducing polynomial particle shape functions for meshfree particle methods, Comput. Methods Appl. Mech. Eng. 196 (35–36) (2007) 3435–3461.
[5] C.A. Duarte, J.T. Oden, An h-p adaptive method using clouds, Comput. Methods Appl. Mech. Eng. 139 (1–4) (1996) 237–262.
[6] N. Moës, J. Dolbow, T. Belytschko, A finite element method for crack growth without remeshing, Int. J. Numer. Methods Eng. 46 (1) (1999) 131–150.
[7] J. Dolbow, N. Moës, T. Belytschko, Discontinuous enrichment in finite elements with a partition of unity method, Finite Elements Anal. Des. 36 (3–4) (2000) 235–260.
[8] T. Strouboulis, K. Copps, I. Babuška, The generalized finite element method, Comput. Methods Appl. Mech. Eng. 190 (January) (2001) 4081–4193.
[9] W.T. Hong, P.S. Lee, Development of flat-top partition of unity method for 2d singular problems, in: OSE (Ocean Systems Engineering) REPORT, 2012.
[10] H.S. Oh, J.G. Kim, W.T. Hong, The piecewise polynomial partition of unity functions for the generalized finite element methods, Comput. Methods Appl. Mech. Eng. 197 (45–48) (2008) 3702–3711.
[11] H.S. Oh, J.W. Jeong, W.T. Hong, The generalized product partition of unity for the meshless methods, J. Comput. Phys. 229 (5) (2010) 1600–1620.
[12] H. Oh, C. Davis, J. Jeong, Meshfree particle methods for thin plates, Comput. Methods Appl. Mech. Eng. 209–212 (0) (2012) 156–171.
[13] W. Cai, H. Lee, H.S. Oh, Coupling of spectral methods and the p-version of the finite element method for elliptic boundary value problems containing singularities, J. Comput. Phys. 108 (2) (1993) 314–326.
[14] K. Shibanuma, T. Utsunomiya, Reformulation of XFEM based on PUFEM for solving problem caused by blending elements, Finite Elements Anal. Des. 45 (11) (2009) 806–816.
[15] C. Johnson, J.-C. Nédélec, On the coupling of boundary integral and finite element methods, Math. Comp. 35 (152) (1980) 1063–1079.
[16] O.C. Zienkiewicz, D.W. Kelly, P. Bettess, The coupling of the finite element method and boundary solution procedures, Int. J. Numer. Methods Eng. 11 (2) (1977) 355–375.
[17] L. Hong-Bao, H. Guo-Ming, H.A. Mang, P. Torzicky, A new method for the coupling of finite element and boundary element discretized subdomains of elastic bodies, Comput. Methods Appl. Mech. Eng. 54 (2) (1986) 161–185.
[18] T. Belytschko, D. Organ, Y. Krongauz, A coupled finite element–element-free Galerkin method, Comput. Mech. 17 (1995) 186–195.
[19] D. Hegen, Element-free Galerkin methods in combination with finite element approaches, Comput. Methods Appl. Mech. Eng. 135 (1–2) (1996) 143–166.
[20] A. Huerta, S. Fernández-Méndez, Enrichment and coupling of the finite element and meshless methods, Int. J. Numer. Methods Eng. 48 (11) (2000) 1615–1636.
[21] H. Karutz, R. Chudoba, W. Krtzig, Automatic adaptive generation of a coupled finite element/element-free Galerkin discretization, Finite Elements Anal. Des. 38 (11) (2002) 1075–1091.
[22] T. Fries, H. Matthies, Coupling meshfree methods and FEM for the solution of the incompressible Navier–Stokes equations, Proc. Appl. Math. Mech. 4 (2004).
[23] I. Babuška, U. Banerjee, J.E. Osborn, On principles for the selection of shape functions for the generalized finite element method, Comput. Methods Appl. Mech. Eng. 191 (49–50) (2002) 5595–5629.
[24] T. Strouboulis, I. Babuška, K. Copps, The design and analysis of the generalized finite element method, Comput. Methods Appl. Mech. Eng. 181 (January) (2000) 43–69.
[25] T. Strouboulis, L. Zhang, I. Babuška, Generalized finite element method using mesh-based handbooks: application to problems in domains with many voids, Comput. Methods Appl. Mech. Eng. 192 (28–30) (2003) 3109–3161.
[26] H.S. Oh, J.G. Kim, J.W. Jeong, The smooth piecewise polynomial particle shape functions corresponding to patch-wise non-uniformly spaced particles for meshfree particle methods, Comput. Mech. 40 (3) (2007) 569–594.
[27] P. Beckers, H. Zhong, E. Maunder, Numerical comparison of several a posteriori error estimators for 2d stress analysis, Eur. J. Finite Element Method 2 (1993).
[28] E. Gdoutos, Fracture Mechanics: An Introduction, Kluwer Academic Publisher, 1993.
[29] P.S. Lee, K.J. Bathe, Development of MITC isotropic triangular shell finite elements, Comput. Struct. 82 (11–12) (2004) 945–962.
[30] P.S. Lee, K.J. Bathe, The quadratic MITC plate and MITC shell elements in plate bending, Adv. Eng. Software 41 (5) (2010) 712–728.
[31] Y. Lee, K. Yoon, P.S. Lee, Improving the MITC3 shell finite element by using the Hellinger–Reissner principle, Comput. Struct. 110–111 (0) (2012) 93–106.
[32] T. Rabczuk, G. Zi, A meshfree method based on the local partition of unity for cohesive cracks, Comput. Mech. 39 (2007) 743–760, http://dx.doi.org/10.1007/s00466-006-0067-4.
[33] T. Rabczuk, G. Zi, A. Gerstenberger, W.A. Wall, A new crack tip element for the phantom-node method with arbitrary cohesive cracks, Int. J. Numer. Methods Eng. 75 (5) (2008) 577–599.
[34] T. Chau-Dinh, G. Zi, P.S. Lee, T. Rabczuk, J.-H. Song, Phantom-node method for shell models with arbitrary cracks, Comput. Struct. 9293 (0) (2012) 242–256.
[35] H.S. Oh, I. Babuška, The method of auxiliary mapping for the finite element solutions of elasticity problems containing singularities, J. Comput. Phys. 121 (2) (1995) 193–212.